Role of the *b* value in quantifying the Size Distribution of Aftershocks

Chun Hui[1,2,3], Changxiu Cheng[1,2,3*], Shi Shen[1,2,3], Jing Yang [4], Peichao Gao [1,2,3]

[1] Key Laboratory of Environmental Change and Natural Disaster, Beijing Normal University, China, 100875

[2] State Key Laboratory of Earth Surface Processes and Resource Ecology, Beijing Normal University, China, 100875

[3] Faculty of Geographical Science, Center for Geodata and Analysis, Beijing Normal University, China, 100875

[4] College of data science, Taiyuan University of Technology, China, 030024

Chun Hui	Beijing, China	201831051038@mail.bnu.edu.cn
Changxiu Cheng	Beijing, China	chengcx@bnu.edu.cn
Shi Shen	Beijing, China	shens@bnu.edu.cn
Jing Yang	Taiyuan, China	yangj@mail.bnu.edu.cn
Peichao Gao	Beijing, China	gaopc@bnu.edu.cn

Corresponding author: Changxiu Cheng

Abstract

This article objectively estimates the spatiotemporal evolution of *b* values before and after two large earthquakes during 2000-2019 along the Longmenshan fault. We apply the Akaike information criterion to statistically assess the temporal variation in *b* values and use the *b* value time series behavior as a tool to quantify the effect of a mainshock on the size distribution of aftershocks. The *b* values in the source regions exhibited decreasing trends prior to two large earthquakes on 12 May 2008 (M_S 8.0) and 20 April 2013 (M_S 7.0). Moreover, the times required for the *b* values to return to a stable state after both mainshocks were basically equivalent to the times taken for aftershocks depth images to cease to change visibly (approximately 1 year following the M_S 8.0 event and approximately 10 months following the M_S 7.0 event). Our results have substantial implications for assessing the hazards of aftershock sequences.

Plain Language Summary

The most noticeable phenomenon by which large earthquakes can significantly change the regional stress state is the aggregation of aftershocks. However, few studies have quantified the size distributions of aftershocks and applied those distributions to earthquake hazard assessments. In this work, we apply the *b* value time series behavior, which is sensitive to changes in stress, to two well-recorded sequences initiated by large earthquakes on 12 May 2008 (M_S 8.0) and 20 April 2013 (M_S 7.0) along the Longmenshan fault. We find that the times aftershocks directly related to the mainshocks (approximately 1 year following the M_S 8.0 event and approximately 10 months following the M_S 7.0 event), which are fully consistent with the times taken for aftershocks depth images to cease to change visibly. Additionally, we discover clear decreasing trends for the *b* values prior to both major earthquakes.

Keywords: *b* value; Akaike information criterion; aftershock; focal depth

1. Introduction

Understanding both the physical mechanism responsible for and the statistical characteristics of the interactions between earthquakes is of great significance for earthquake hazard. It is widely accepted that earthquakes interact with each other by changing the states of static and dynamic stresses in their surroundings (Stein, 1999). The most noticeable consequence of such a stress change is a dramatic increase in the rate of seismicity, which in most cases is considered an aftershock phenomenon (Ebel et al., 2000). Statistically, reduced aftershock activity is classically described by $K/(t + c)$, where K and c are constants that describe the aftershock productivity and delay time, respectively (Omori, 1894; Utsu et al., 1995). In this context, Ogata (1988,1998) described how aftershock activity is a component of a cascading or branching process and proposed the epidemic-type aftershock sequence model, which is the best currently available statistical description of seismicity (Marzocchi et al., 2017).

However, changes in stress can impact not only the seismicity rate but also the frequency size distribution, alternatively known as the frequency-magnitude distribution (FMD), of subsequent earthquakes (Gulia et al.,2018). An FMD, as its name implies, typically describes the relationship between the magnitude and frequency of earthquakes; this relationship is commonly known as the Gutenberg-Richter (G-R) law (Gutenberg and Richter,1944), expressed as $logN=a-bM$, where N is the cumulative number of events above magnitude M, a describes the productivity, and b signifies the average size distribution of those earthquakes. According to global statistics, the b value of a large seismic area is generally close to 1.0 (Evernden, 1970; Lay and Wallce, 1995), but variations in b values do occur regionally; these variations are highly correlated with the regional characteristics of seismic activity and may be significant, for example, ranging from 0.5 to 1.3 near Parkfield on the San Andreas fault (Schorlemmer et al., 2004) or from 0.5 to 1.5 in California and Japan (Turcotte, 1986; Ogata and Katsura, 1993).

The variation in the b value is sensitive to the differential stress (Gulia and Wiemer, 2019). Previous studies have confirmed that the b value is inversely dependent on the differential stress in both the laboratory (Amitrano, 2003; Goebel et al., 2013) and the field (Varotsos et al., 2013; Sarlis et al, 2013). A region with a low b value is implied to exhibit a large differential stress, suggesting its being toward the end of the seismic cycle (Schorlemmer et al., 2005). Such a relationship can be used as a precursor for earthquake forecasting (Gulia and Wiemer, 2019; Xie et al,.2019). One study on a series of 58 aftershock sequences from California, Japan, Italy and Alaska showed that the b value of an aftershock sequence generally increases after the mainshock by 20-30% (Gulia et al.,2018). Scholz (2019) defined aftershocks as typically beginning immediately following the mainshock over the entire rupture area and its surroundings and confined aftershocks to locations where large stress concentrations have been produced by a mainshock rupture. However, all large crustal earthquakes are followed by a decaying aftershock sequence that typically lasts for months to years, and no scientific means have been developed to prospectively quantify the 'classic' aftershock sequences following different types of large crustal earthquakes.

A recent topic of ongoing debate has been whether the 2013 M_S 7.0 Lushan earthquake was a strong aftershock of the 2008 M_S 8.0 Wenchuan earthquake or a new and independent event. For example, Li et al. (2014) inferred that the Lushan earthquake was an independent mainshock rather than an aftershock of the Wenchuan earthquake because different faults sourced the two events, although both faults were situated within the same Longmenshan fold-and-thrust belt. Many other researchers, such as Zhang et al. (2013) and Xu et al. (2013), similarly postulated that the Lushan earthquake was a new event because the ruptures produced by the Wenchuan and Lushan events do not overlap with each other. The opposing belief is that the Lushan earthquake was a strong aftershock of the Wenchuan earthquake. For instance, Zhu (2016) analyzed the statistical properties of the Wenchuan-Lushan earthquake sequence and showed that the Lushan event can be regarded as one of many aftershocks following the Wenchuan mainshock that satisfy the empirical laws of aftershocks. Furthermore, Parsons and Segou (2014) and Wang et al. (2014) also reported that the Lushan event was triggered by the Wenchuan event and should thus be regarded as a delayed aftershock.

Nevertheless, the above results were based mostly upon phenomenological and theoretical analyses, which are characterized by very strong uncertainties and randomness. In addition, these studies focused more on the characteristics of the two major earthquakes rather than on the subsequent earthquakes directly related to the two events.

To date, systematic research has not been performed on the effect of a mainshock's differential stress change on the size distribution of related aftershocks (Ogata & Katsura, 2014; Tamaribuchi et al., 2018; Gulia et al.,2018). However, individual case studies have shown that lower *b* values are occasionally observed before a mainshock and that higher *b* values are sometimes observed after a mainshock (Shi et al.,2018; Xie et al,.2019; Li et al., 2018). These observations highlight valuable questions, namely, whether, when and how such changes in the *b* value are recovered. Accordingly, for the first time, we assume that when there is no large earthquake, the b value in an area is stable for a long time, and the disturbance of a large earthquake will change this state temporarily. So we evaluate the behaviors of *b* values before and after mainshocks to quantify the size distribution of aftershocks to facilitate the application of results to earthquake hazard assessments in the future.

In this work, we take the seismic catalog of the M_S 8.0 Wenchuan earthquake and the M_S 7.0 Lushan earthquake (which possess the most abundant aftershock sequences to date) as an example. Our research includes three main sections: section one tests the research data, that is, the completeness of the earthquake catalog; section two analyzes the spatiotemporal evolution of *b* values before and after these two large earthquakes in the study area; and section three verifies the results by using the Akaike information criterion (AIC) and aftershock depth images.

2. Earthquake catalog

In this work, we use the earthquake catalog recorded by the China Earthquake Networks Center (CENC) during the period from 1 January 2000 to 1 January 2019. The earthquake monitoring capability of the CENC has been greatly enhanced since 2000 (Liu et al.,2003). Two large earthquakes with magnitudes greater than 7 struck the study area during the study period on 12 May 2008 (M_S 8.0) and 20 April 2013 (M_S 7.0).

To evaluate the reliability of the catalog, we test its completeness by calculating the completeness magnitude, M_C, defined as the minimum magnitude at which the cumulative FMD departs from the decay trend (Mignan, 2011). Many techniques that focus on the estimation of M_C follow the validity of the G-R law; examples include the goodness-of-fit test (Gao and Gao,2002), the entire magnitude range technique (Ogata and Katsura, 1993), and the maximum curvature (MAXC) method (Wiemer and Wyss, 2000).

In the present work, we use the MAXC technique because it is a robust and straightforward method for estimating M_C by finding the magnitude bin with the highest frequency of events in the FMD plot. However, the MAXC technique has been shown to underestimate M_C in cases involving gradually curved FMDs; Mignan (2011) postulated that this underestimation tendency arises from spatiotemporal heterogeneities within the network. Therefore, we use the MAXC method and add a correction factor of +0.2 (Woessner and Wiemer,2005, Gulia and Wiemer, 2019). According to the evaluation result, we select events with magnitudes $M \geq M_C$=1.5.

3. Methods

3.1. Estimation of the *b* value

The least square method and maximum likelihood estimation are often used to calculate the *b* value; between them, the latter approach is considered more stable. In this work, we use maximum likelihood estimation to estimate the *b* value and the standard deviation (Aki, 1965; Utsu, 1965):

$$b = \frac{1}{\ln(10)(\overline{M} - M_C)}$$

where $\overline{M}$ denotes the average magnitude of a set of earthquakes with $M \geq M_C$ and M_C is the magnitude of completeness. In addition, the standard deviation (σ) of the *b* value is expressed as follows:

$$\sigma = \frac{b}{\sqrt{N}}$$

where *N* is the number of events used for the *b* value estimation.

3.2. Statistical assessment of *b* value changes

Here, the AIC (Akaike, 1974) is used to test whether the temporal change in the *b* value is significant. We compare the *AIC* values for two sample time windows with different *b* values (b_1 and b_2), leading to the difference *ΔAIC* (Utsu,1992):

$$\Delta AIC = -2(N_1 + N_2)\ln(N_1 + N_2) + 2N_1 \ln(N_1 + \frac{N_2 b_1}{b_2}) + 2N_2 \ln(N_2 + \frac{N_1 b_2}{b_1}) - 2$$

where N_1 and N_2 are the number of events in each sample and b_1 and b_2 are the *b* value of each sample time window. In this approach, P_b is defined as the probability of the hypothesis that the *b* values of the two sample time windows originate from the same population. P_b is derived from the AIC as follows:

$$P_b = e^{(-\Delta AIC/2)-2}$$

Utsu (1992) defined the difference between two *b* values as nonsignificant when $\Delta AIC<2$ ($P_b \approx 0.05$), whereas the difference is considered highly significant when $\Delta AIC>5$ ($P_b \approx 0.01$).

4. Results

In this study, we investigate the distributions of *b* values before and after two large events that occurred during 2000-2019 along the Longmenshan fault. However, computing reliable space-time series of the *b* value is difficult because the consistency and quality of an earthquake catalog are strongly affected by changes in the seismic network during the detection period. Therefore, we select only events with $M \geq M_C$=1.5 and use a time window and spatial grid to calculate the *b* values.

Figures 1a and 1b display the temporal variations in the *b* values for the two regions studied. In this computation, the window lengths are set to at least 500 events and 200 events. Each window is moved forward by one event at a time. The *b* values show a decreasing trend before the occurrence of both large earthquakes in both regions. To ensure that this trend is statistically significant, we quantitatively assess the temporal variation in the *b* values using the *P* parameter test and select 3 windows before the M_S 8.0 event (W_1, W_2 and W_3) and before the M_S 7.0 event (L_1, L_2 and L_3) (Fig. 1a, b). The results are shown in Table 1.

Table 1 The results of the *P* parameter test

Windows	*ΔAIC*	P_b
W_{12}	3.8	0.02

W_{23}	3.2	0.03
W_{13}	19.9	6.4×10^{-6}
L_{12}	2.6	0.03
L_{23}	4.6	0.01
L_{13}	20	5.9×10^{-6}

Utsu (1992) also defined the statistical significance of the change in the *b* value in terms of the *P* parameter, which counts the percentage of $\Delta AIC \geq 2$. Table 1 shows that the *b* values decreased before both large earthquakes with statistically significant variations.

After the Wenchuan M_S 8.0 event, the *b* values in the Wenchuan source area increased quickly and then underwent a period of rapid fluctuation (indicated by the pink shading lasting not more than 1 year) before gradually approaching a period of small oscillation (Fig. 1a). This last period of minor fluctuation is similar to the FMD in the third period (Fig. 1c, *b*=0.84). In contrast, after the Lushan M_S 7.0 event, the *b* values in the Lushan source area increased rapidly and then slowly dropped to a steady state (Fig. 1b), almost similar to the FMD in the first period (Fig. 1d, *b*=0.76). As shown in Figure 1b (red shading), the *b* value required less than 10 months to return to a stable state.

If we estimate reference *b* values for the background levels (for the period, *b*=1.03 in the Wenchuan source region, while *b*=0.76 in the Lushan source region), the results indicate that no large earthquake occurred in either region. Evidently, when the *b* value is basically stable, the *b* values in the Lushan source area essentially return to the background level (*b*=0.76), whereas those in the Wenchuan source area drop beyond the background level (from 1.03 to 0.84). No large event has occurred since the Lushan earthquake in either region.

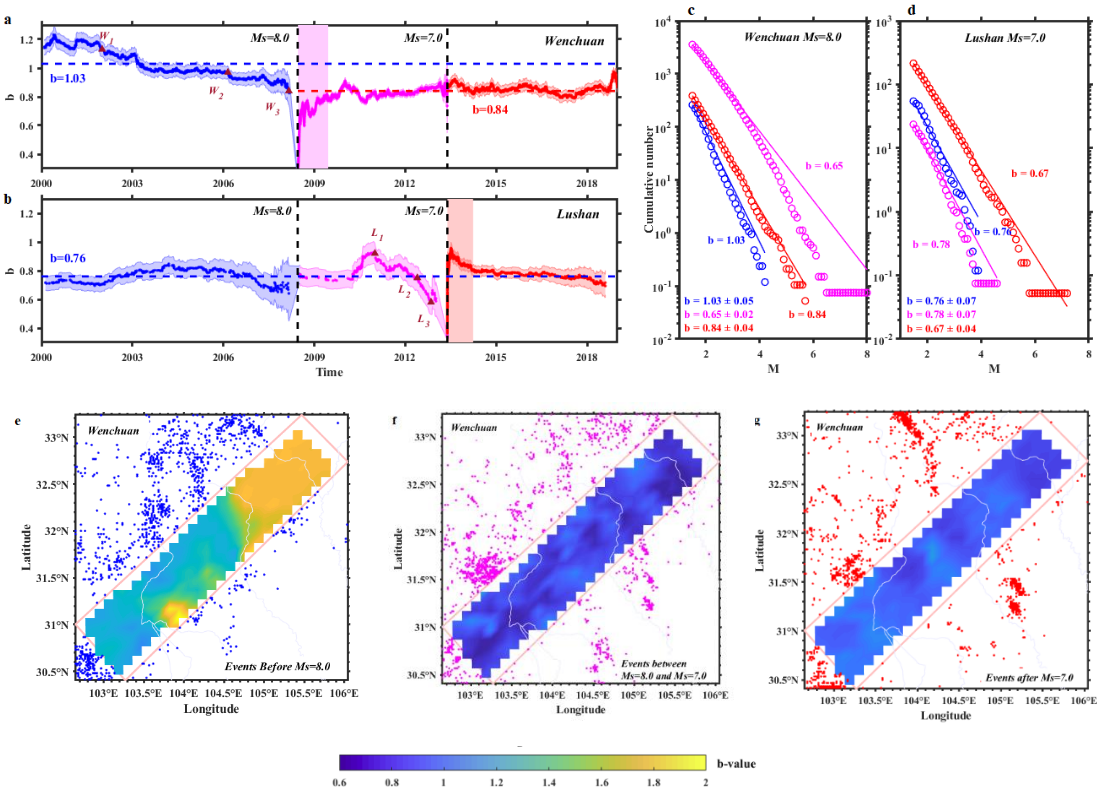

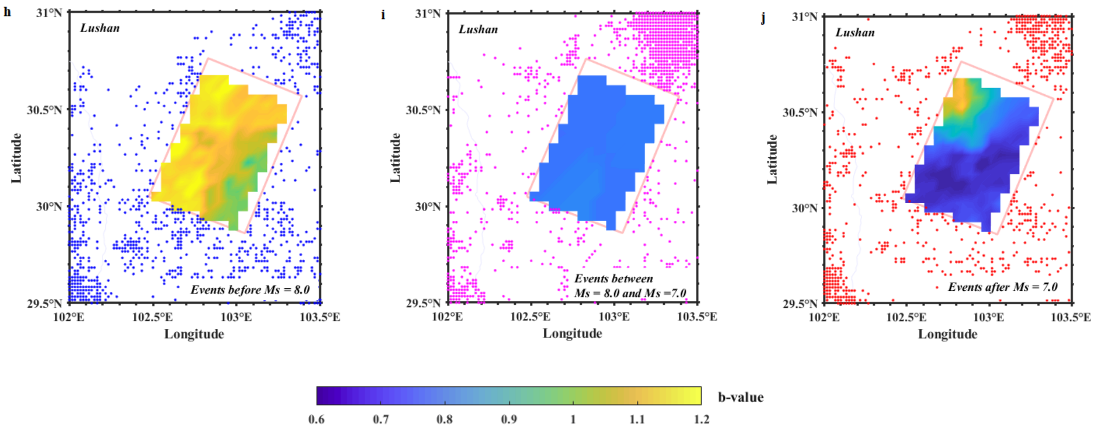

Figure 1. Time-space analysis of the *b* values for the Wenchuan-Lushan sequence

a, **b**, Time series of *b* values for the source regions of the Wenchuan and Lushan mainshocks. The two dashed black lines represent the occurrence times of the M_S=8.0 (Wenchuan) and M_S=7.0 (Lushan) events, and the dashed blue lines represent the *b* values before the two mainshocks. The dashed red lines represent the *b* values after the occurrence time of the M_S=7.0 (Lushan). The shaded areas represent the uncertainties in the *b* values. **c**, **d**, Frequency-magnitude distributions for the two source regions in three different periods. **e**, **f**, **g**, Spatial distributions of the *b* value for the Wenchuan region in three different periods. **h**, **i**, **j**, Spatial distributions of the *b* value for the Lushan region in three different periods.

To analyze the spatial footprints of the changes in the *b* values, we divide the two study regions into 0.1°×0.1° grids, sample the 300 events nearest to each grid node, up to a maximum radius of 25 km, and re-estimate the magnitude of completeness in each node; for this purpose, we randomly sampled the events 1000 times (bootstrap approach). Then, we calculate the regional *b* values for all events with M_L≥1.5. The results are very consistent with the time series analysis (Fig. 1a, b) and FMDs (Fig. 1c, d). Figures 1e-1f demonstrate the spatial variation in the *b* values throughout the Wenchuan source region. In the period between the M_S=8.0 and M_S=7.0 mainshocks, the *b* values decrease over the whole region, especially in the northeast (Fig. 1f), and the distribution changes slightly after the M_S=7.0 Lushan event (Fig. 1g). These findings reveal that the seismicity within the Wenchuan source region was barely influenced by the Lushan M_S 7.0 event.

Figures 1h-1j show the spatial variation in the *b* values in the Lushan source region. The distribution of *b* values changes markedly after the M_S=8.0 event, with the *b* values decreasing significantly in the Lushan source region (Fig. 1i). Five years later, with the occurrence of the M_S=7.0 Lushan event, the *b* values decreased slightly in most regions (Fig. 1j). This *b* value analysis thus suggests that the Wenchuan M_S 8.0 mainshock strongly influenced the stress level within the Lushan source region and may have contributed to the occurrence of the M_S=7.0 Lushan event. However, this result is not entirely consistent with the time series analysis results of the *b* values described above (Fig. 1b), and the shape of the time series changes very little. This space-time inconsistency may be explained simply that the Wenchuan M_S 8.0 event changed the stress level in the Lushan source region but had little impact on the rate of seismicity therein.

5. Discussion

From recent analyses of seismicity (Varotsos et al., 2013; Sarlis et al, 2013; Shi et al.,2018;

Xie et al,.2019), a temporal decrease in the *b* value before a large earthquake could be a forecasting indicator. Our investigation reveals a decrease in the *b* values before the M_S 8.0 and M_S 7.0 earthquakes (Fig. 1a, b), but these temporal variations may occur over a timescale ranging from months to years. Consequently, the timeliness and effectiveness of this variability as an indicator are hard to guarantee. In addition, there is usually an insufficient number of events to accurately calculate the *b* values before large earthquakes. Regarding the abundance of seismic data, Gulia and Wiemer (2019) pointed out that the period following a moderate earthquake is rich in such data, with thousands of events occurring within a short period of time. These events may allow real-time monitoring of the evolution of *b* values and the discrimination of whether an ongoing sequence represents foreshocks preceding an upcoming large event.

There is considerable uncertainty about whether sufficient foreshocks occur before a large earthquake, but it is widely accepted that the stage of the earthquake cycle after a large earthquake is characterized by thousands of aftershocks. This aftershock activity can be effectively described through statistics; however, the equally fundamental effect of a mainshock on the size distribution of aftershocks has still not been quantified and is therefore not used in earthquake hazard assessments (Gulia et al.,2018). In addition, Gulia et al. (2018) pointed out that Coulomb stress change models and operational aftershock forecasting models such as the epidemic-type aftershock sequence model (Ogata, 1988, 1999) and short-term earthquake probability (STEP) model (Gerstenberger et al., 2005) forecast a high probability for a mainshock rupture to repeat and thus substantially overestimate the aftershock hazard. This may also be partly because no scientific consensus has been reached on the exact definition of an aftershock. Kisslinger (1996) divided aftershocks into the following three classes: class 1 aftershocks occur on the same section of the fault surface that slipped during the mainshock; class 2 aftershocks occur on the same fault that ruptured to generate the mainshock but are located outside the section of initial slip; and class 3 aftershocks occur on faults other than the seismogenic fault that produced the mainshock but were presumably triggered by the mainshock. A basic definition of an aftershock is that the barriers that remain unbroken during a mainshock are natural sites of stress concentration and thus signify the sources of aftershocks (Das and Aki ,1977). Based on this basic definition, after a mainshock, it takes some time for the regional tectonic stress to return to a stable state, which can be measured by the change in *b* values (Li et al., 2018).

Therefore, we propose that the decay time of a classic aftershock sequences can be quantified by assuming a stable state of the *b* value before and after a large earthquake and by delimiting the period of dramatic variation in the *b* value. In this work, we estimate reference *b* values for the background levels (stable states) in both regions, and no large earthquakes are considered to occur in the region. Then, according to the evolution of the *b* values over time, another stable state of the *b* value is observed. The results show that it takes approximately 1 year for the *b* value in the Wenchuan source region to return to another stable state (Fig. 1a, c) and approximately 10 months for the *b* value in the Lushan source region to return to its original stable state (Fig. 1b, d).

To verify the reliability of these findings, we use the focal depth data of the aftershocks following each mainshock to spatially scan the study area and divide the region into 0.1°×0.1° grids; then, we calculate the average of all event depths in each grid to represent the depth of the lattice points and apply kriging interpolation to all the grids. We sample the 10 events nearest to each grid node in the Wenchuan source region in case the average depth of the lattice point is affected by too few events. The results are shown in Figure 2, in which we depict the evolution of the deep seismogenic and tectonic environment in the aftershock area and provide depth images of the spatial evolution of the aftershocks at 1 day, 1 week, 1 month, 6 months, 1 year and 3 years after the mainshock. The aftershock focal depth-activity images 1 year and 3 years after the mainshock indicate that the aftershock pattern did not change in the 3 years following the main event, suggesting that aftershock activities directly related to the mainshock basically cease within 1 year. This finding implies that the stress adjustment process of the mainshock in this region lasted almost for approximately 1 year, which is basically consistent with the abovementioned time required for the *b* value to return to a stable state. The same calculation process was repeated in the Lushan source region, and the results revealed that the aftershock focal depth did not change significantly after 10 months subsequent to the mainshock (Fig. 3).

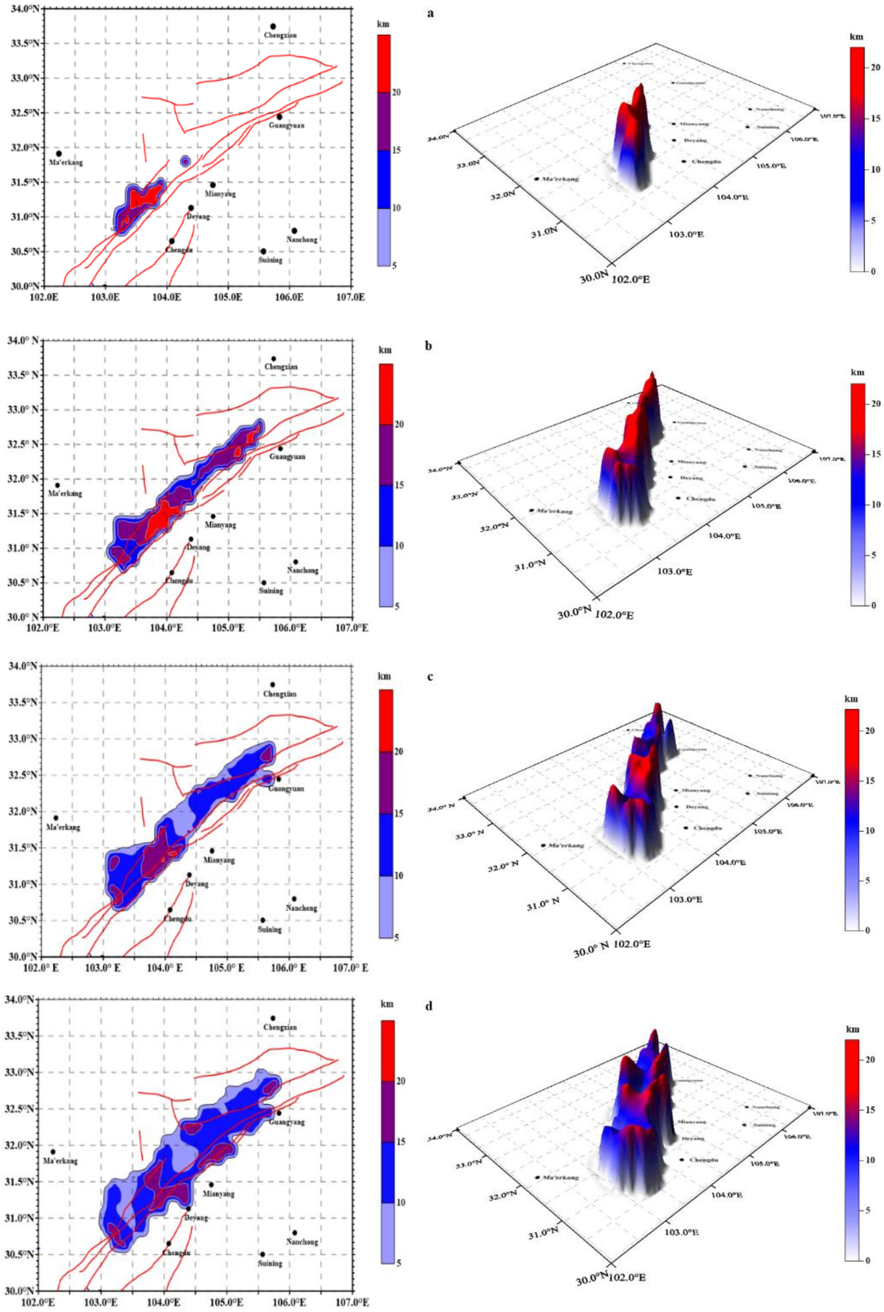

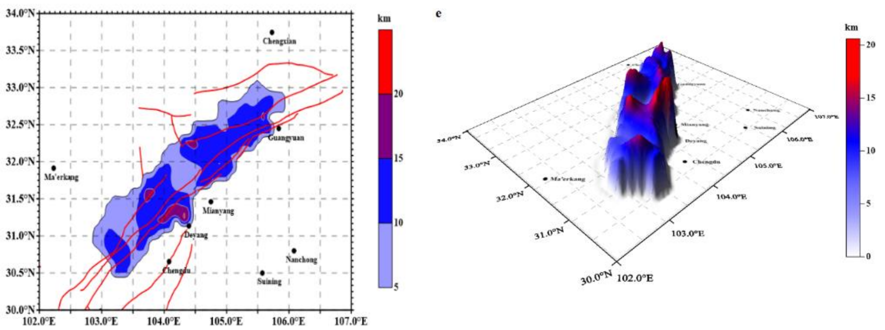

Figure 2. Spatial distribution of the focal depths of the aftershocks following the Wenchuan M_S 8.0 earthquake on the fault plane Red lines represent the locations of faults. **a** One day after the mainshock; **b** 1 week after the mainshock; **c** 1 month after the mainshock; **d** 1 year after the mainshock; **e** 3 years after the main shock.

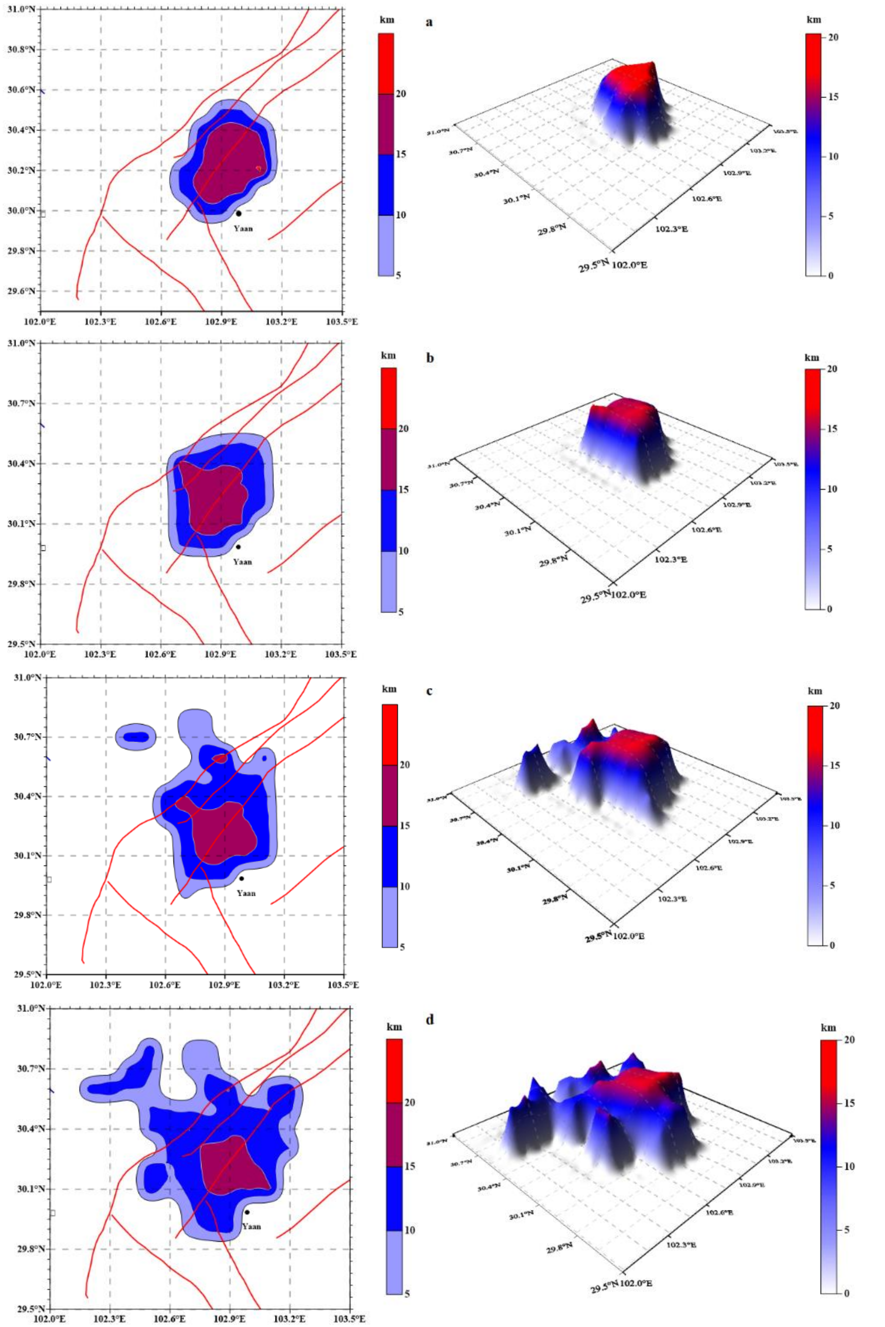

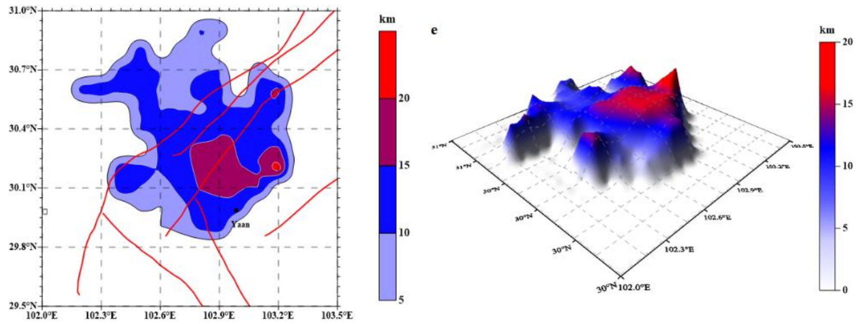

Figure 3. Spatial distribution of the focal depths of the aftershocks following the Lushan M_S 7.0 earthquake on the fault plane Red lines represent the locations of faults. **a** One day after the mainshock; **b** 1 month after the mainshock; **c** 5 months after the mainshock; **d** 10 months after the mainshock; **e** 2 years after the mainshock.

6. Conclusion

Based on the fracture characteristics and potential seismicity surrounding the source regions of the Wenchuan M_S 8.0 and Lushan M_S 7.0 earthquakes, we use *b* value time series to verify the reliability of the *b* value as a precursor for large earthquakes. The results depict clear decreasing trends of *b* values prior to two major large earthquakes in the analyzed area. Additionally, the results of a *P* parameter test demonstrate that the decreasing trend is statistically significant ($\Delta AIC \geq 2$).

In addition, we assume that the b value in an area will be stable for a long time without large earthquake disturbance, and then we establish that the variation in the *b* value behaves transiently over time. The results showed that after the mainshock, the *b* value in the Wenchuan source region took approximately 1 year to drop to another stable state (*b* values ranging from 1.03 to 0.84), while the *b* value in the Lushan source region took approximately 10 months to return (almost) to its original stable state (b=0.76). Focal depth images of the aftershocks also show that the aftershock distributions were directly related to the mainshocks of the Wenchuan M_S 8.0 and Lushan M_S 7.0 earthquakes within 1 year and 10 months, respectively. So we propose that the variations in *b* values are impermanent over time and can be used as a tool to quantify the effect of a mainshock on the size distribution of aftershocks.

Moreover, the results of spatial analysis reveal that the *b* value in the Lushan source region decreased after the M_S 8.0 event; however, the *b* value time series indicate that the Wenchuan M_S 8.0 event had almost no significant impact on the Lushan source region. Therefore, we support the view that the Wenchuan M_S 8.0 earthquake and Lushan M_S 7.0 earthquake were two independent events.

Acknowledgments and Data

This research was supported by the National Natural Science Foundation of China (Grant No. 41771537) and the Fundamental Research Funds for the Central Universities. And thank the American Journal Experts(AJE) for polishing the language of this article. No conflict of interest exits in the submission of this manuscript, and manuscript is approved by all authors for publication.

The earthquake catalog for this article are from the China Earthquake Networks Center (CENC, http://www.cenc.ac.cn/). All our data is open source.

References

Akaike, H. (1974). A new look at the statistical model identification. In *Selected Papers of Hirotugu Akaike*, 215-222. Springer.

Aki, K. (1965) Maximum likelihood estimate of b in the formula log N= a-bM and its confidence limits. *Bull. Earthq. Res. Inst., Tokyo Univ.,* 43**,** 237-239.

Amitrano, D. (2003) Brittle-ductile transition and associated seismicity: Experimental and numerical studies and relationship with the b value. *Journal of Geophysical Research: Solid Earth,* 108.

Cao, A. & Gao, S. S. (2002) Temporal variation of seismic b-values beneath northeastern Japan island arc. *Geophysical research letters,* 29**,** 48-1-48-3.

Das, S. & Aki, K. (1977) Fault plane with barriers: a versatile earthquake model. *Journal of geophysical research,* 82**,** 5658-5670.

Ebel, J. E., Bonjer, K. P. & Oncescu, M. C. (2000) Paleoseismicity: Seismicity evidence for past large earthquakes. *Seismological Research Letters,* 71**,** 283-294.

Evernden, J. (1970) Study of regional seismicity and associated problems. *Bulletin of the Seismological Society of America,* 60**,** 393-446.

Gerstenberger, M. C., Wiemer, S., Jones, L. M. & Reasenberg, P. A. (2005) Real-time forecasts of tomorrow's earthquakes in California. *Nature,* 435**,** 328.

Goebel, T. H. W, Schorlemmer, D., Becker, T. W, Dresen, G. & Sammis, C. G. (2013) Acoustic emissions document stress changes over many seismic cycles in stick-slip experiments. *Geophysical Research Letters,* 40**,** 2049-2054.

Gulia, L. & Wiemer, S. (2019) Real-time discrimination of earthquake foreshocks and aftershocks. *Nature,* 574**,** 193-199.

Gulia, L., Rinaldi, A., Tormann, T., Vannucci, G., Enescu, B. & Wiemer, S. (2018) The Effect of a Mainshock on the Size Distribution of the Aftershocks. *Geophysical Research Letters,* 45**,** 13,277-13,287.

Gutenberg, B. & Richter, C. F. (1944) Frequency of earthquakes in California. *Bulletin of the Seismological society of America,* 34**,** 185-188.

Kisslinger, C. (1996) Aftershocks and fault-zone properties. *Advances in geophysics,* 38**,** 1-36.

Lay, T. & Wallace, T. C. 1995. *Modern global seismology*. Elsevier.

Li, L., Adhikari, L. B., Gang, L. & FuWang, G. (2018) Characteristics of temporal-spatial distribution of the aftershocks of the 2008 M (s) 8. 0 Wenchuan Earthquake. *CHINESE JOURNAL OF GEOPHYSICS-CHINESE EDITION,* 61**,** 1797-1805.

Li, Y. Q., Jia, D., Wang, M. M., Shaw, J. H., He, J. K., Lin, A. M., Xiong, L. & Rao, G. (2014) Structural geometry of the source region for the 2013 Mw 6.6 Lushan earthquake: Implication for earthquake hazard assessment along the Longmen Shan. *Earth and Planetary Science Letters,* 390**,** 275-286.

Liu, R. F., Wu, Z. L., Yin, C. M., Chen, Y. T. & Zhuang, C. T. (2003) Development of China digital seismological observational systems. *Acta Seismologica Sinica,* 16**,** 568-573.

Marzocchi, W., Taroni, M. & Falcone, G. (2017) Earthquake forecasting during the complex Amatrice-

Norcia seismic sequence. *Science advances,* 3, e1701239.

Mignan, A., Werner, M. J., Wiemer, S., Chen, C. C. & Wu, Y. M. (2011) Bayesian estimation of the spatially varying completeness magnitude of earthquake catalogs. *Bulletin of the Seismological Society of America,* 101, 1371-1385.

Ogata, Y. (1988) Statistical models for earthquake occurrences and residual analysis for point processes. *Journal of the American Statistical association,* 83, 9-27.

Ogata, Y. (1998) Space-time point-process models for earthquake occurrences. *Annals of the Institute of Statistical Mathematics,* 50, 379-402.

Ogata, Y. & Katsura, K. (1993) Analysis of temporal and spatial heterogeneity of magnitude frequency distribution inferred from earthquake catalogues. *Geophysical Journal International,* 113, 727-738.

Ogata, Y. & Katsura, K. (2014) Comparing foreshock characteristics and foreshock forecasting in observed and simulated earthquake catalogs. *Journal of Geophysical Research: Solid Earth,* 119, 8457-8477.

Omori, F. 1894. *On the after-shocks of earthquakes*. The University.

Parsons, T. & Segou, M. (2014) Stress, distance, magnitude, and clustering influences on the success or failure of an aftershock forecast: The 2013 M 6.6 Lushan earthquake and other examples. *Seismological Research Letters,* 85, 44-51.

Sarlis, N. V., Skordas, E. S., Varotsos, P. A., Nagao, T., Kamogawa, M., Tanaka, H. & Uyeda, S. (2013) Minimum of the order parameter fluctuations of seismicity before major earthquakes in Japan. *Proceedings of the National Academy of Sciences,* 110, 13734-13738.

Scholz, C. H. 2019. *The mechanics of earthquakes and faulting*. Cambridge university press.

Schorlemmer, D., Wiemer, S. & Wyss, M. (2004) Earthquake statistics at Parkfield: 1. Stationarity of b values. *Journal of Geophysical Research: Solid Earth,* 109.

Schorlemmer, D., Wiemer, S. & Wyss, M. (2005) Variations in earthquake-size distribution across different stress regimes. *Nature,* 437, 539.

Shi, H. X., Meng, L. Y., Zhang, X. M., Chang, Y., Yang, Z. T., Xie, W. Y., Hattori, K. & Han, P. (2018) Decrease in b value prior to the Wenchuan earthquake (M (s) 8.0). *CHINESE JOURNAL OF GEOPHYSICS-CHINESE EDITION,* 61, 1874-1882.

Stein, R. S. (1999) The role of stress transfer in earthquake occurrence. *Nature,* 402, 605-609.

Tamaribuchi, K., Yagi, Y., Enescu, B. & Hirano, S. (2018) Characteristics of foreshock activity inferred from the JMA earthquake catalog. *Earth, Planets and Space,* 70, 90.

Turcotte, D. (1986) A fractal model for crustal deformation. *Tectonophysics,* 132, 261-269.

Utsu, T. (1965) A method for determining the value of" b" in a formula log n= a-bM showing the magnitude-frequency relation for earthquakes. *Geophys. Bull. Hokkaido Univ.,* 13, 99-103.

Utsu, T. (1992) Report of the Joint Research Institute for Statistical Mathematics.

Utsu, T. & Ogata, Y. (1995) The centenary of the Omori formula for a decay law of aftershock activity. *Journal of Physics of the Earth,* 43, 1-33.

Varotsos, P., Sarlis, N., Skordas, E. & Lazaridou, M. (2013) Seismic Electric Signals: An additional fact showing their physical interconnection with seismicity. *Tectonophysics,* 589, 116-125.

Wang, Y., Wang, F., Wang, M., Shen, Z. K. & Wan, Y. (2014) Coulomb stress change and evolution induced by the 2008 Wenchuan earthquake and its delayed triggering of the 2013 Mw 6.6 Lushan earthquake. *Seismological Research Letters,* 85, 52-59.

Wiemer, S. & Wyss, M. (2000) Minimum magnitude of completeness in earthquake catalogs: Examples from Alaska, the western United States, and Japan. *Bulletin of the Seismological Society of America,* 90**,** 859-869.

Woessner, J. & Wiemer, S. (2005) Assessing the quality of earthquake catalogues: Estimating the magnitude of completeness and its uncertainty. *Bulletin of the Seismological Society of America,* 95**,** 684-698.

Xie, W. Y., Hattori, K. & Han, P. (2019) Temporal Variation and Statistical Assessment of the b Value off the Pacific Coast of Tokachi, Hokkaido, Japan. *Entropy,* 21**,** 249.

Xu, X. W. & Wen, X. Z. (2013) LushanMS 7.0 Earthquake: A Blind Reserve-FaultEarthquake. *ChineseScienceBulletin,* 58**,** 1887-1893.

Zhang, P. Z. (2008) Slip rates and recurrence intervals of the Longmen Shan active fault zone, and tectonic implications for the mechanism of the May 12 Wenchuan earthquake, 2008, Sichuan, China. *Chinese J. Geophys.,* 51**,** 1066-1073.

Zhang, Y. Q., Dong, S. W., Hou, C. T., Shi, J. S., Wu, Z. H., Li, H. L., Sun, P., Liu, G. & Li, J. (2013) Seismogenic structure of the April 20, 2013, Lushan Ms7 earthquake in Sichuan. *Acta Geologica Sinica-English Edition,* 87**,** 633-645.

Zhu, S. (2016) Is the 2013 Lushan earthquake (Mw= 6.6) a strong aftershock of the 2008 Wenchuan, China mainshock (Mw= 7.9)? *Journal of Geodynamics,* 99**,** 16-26.

Figure.

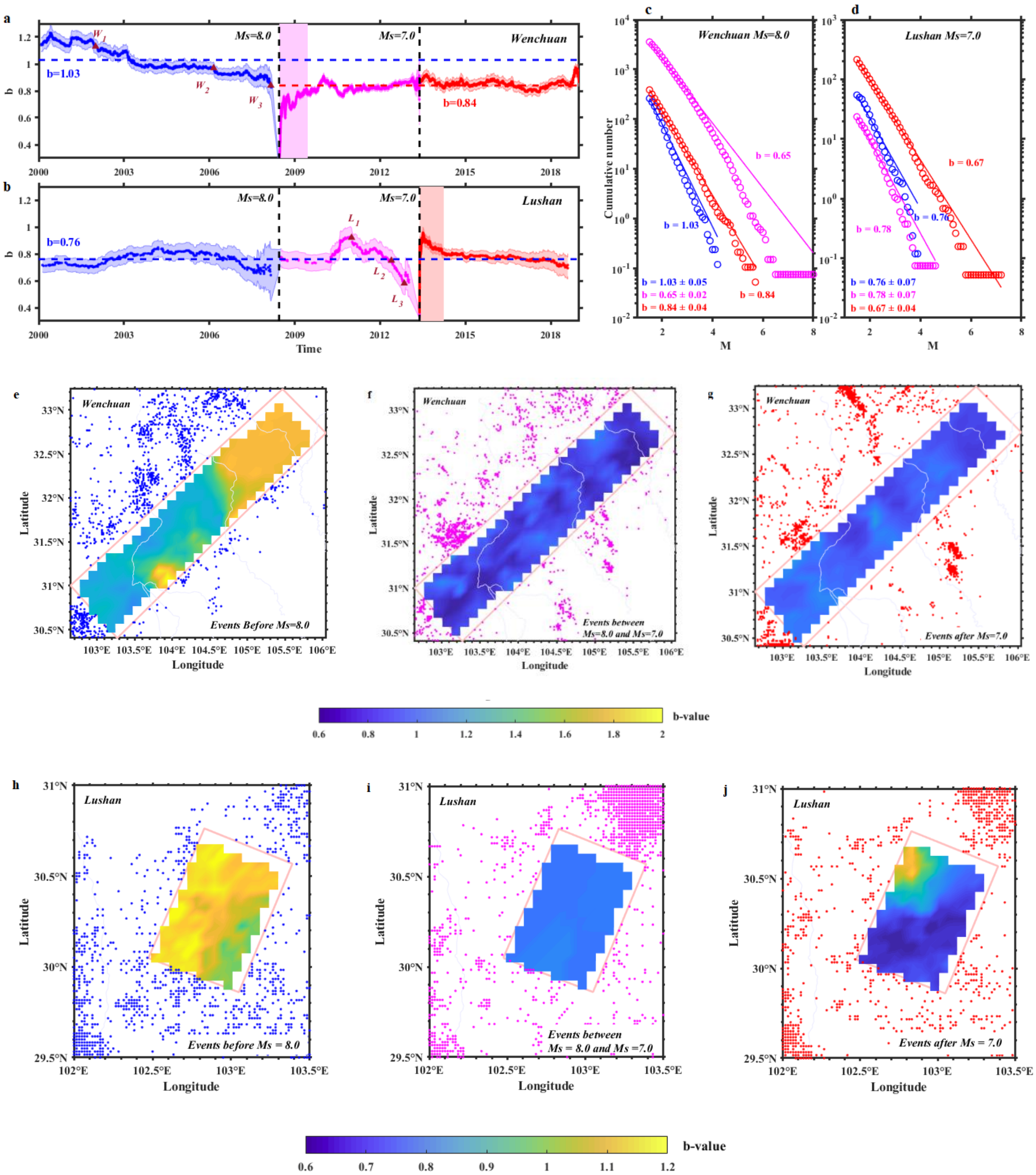

Figure 1. Time-space analysis of the *b* values for the Wenchuan-Lushan sequence

a, **b**, Time series of *b* values for the source regions of the Wenchuan and Lushan mainshocks. The two dashed black lines represent the occurrence times of the M_S=8.0 (Wenchuan) and M_S=7.0 (Lushan) events, and the dashed blue lines represent the *b* values before the two mainshocks. The dashed red lines represent the *b* values after the occurrence time of the M_S=7.0 (Lushan). The shaded areas represent the uncertainties in the *b* values. **c**, **d**, Frequency-magnitude distributions for the two source regions in three different periods. **e**, **f**, **g**, Spatial distributions of the *b* value for the Wenchuan region in three different periods. **h**, **i**, **j**, Spatial distributions of the *b* value for the Lushan region in three different periods.

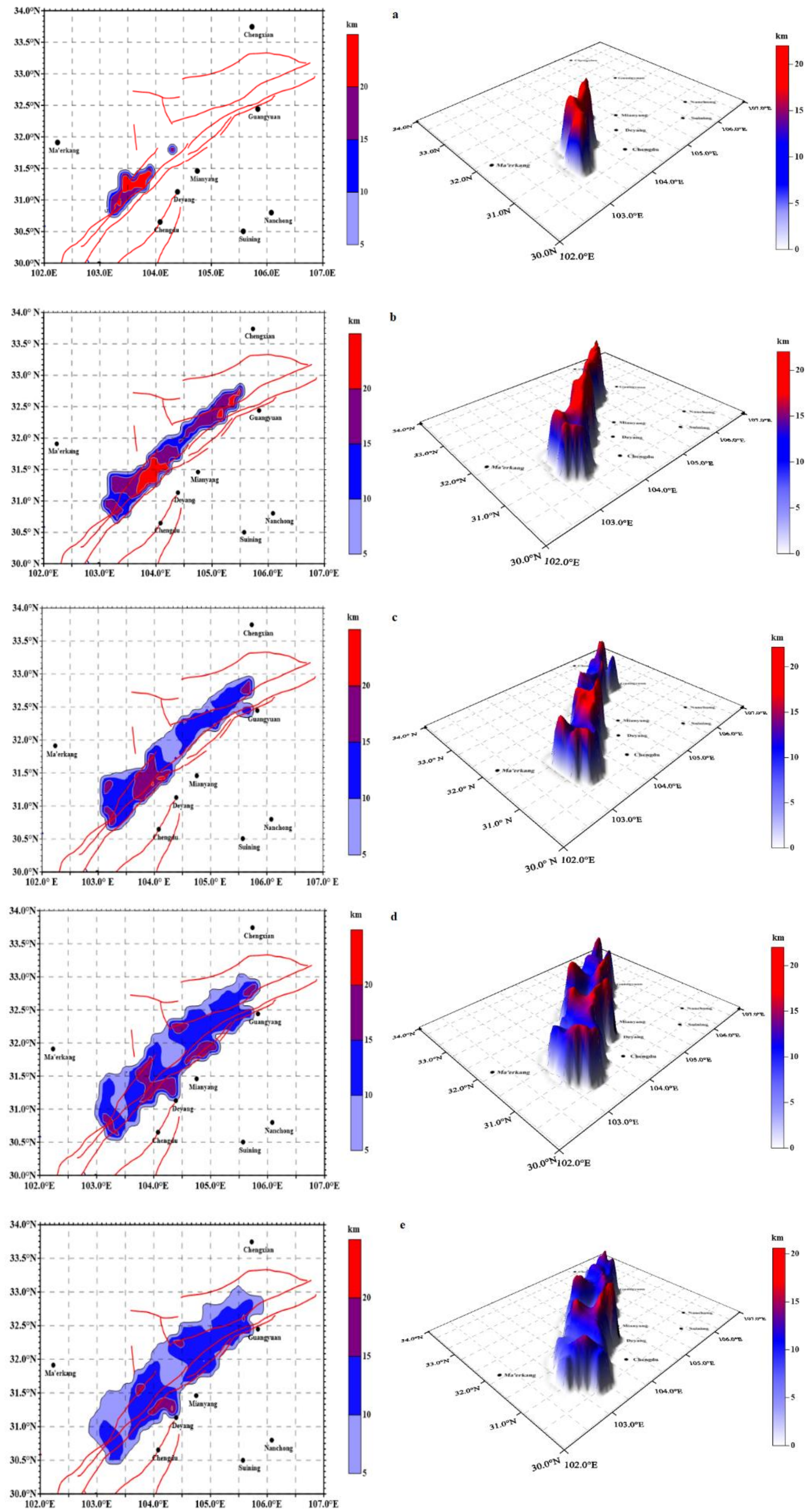

Figure 2. Spatial distribution of the focal depths of the aftershocks following the Wenchuan *Ms* 8.0 earthquake on the fault plane Red lines represent the locations of faults. **a** One day after the mainshock; **b** 1 week after the mainshock; **c** 1 month after the mainshock; **d** 1 year after the mainshock; **e** 3 years after the main shock.

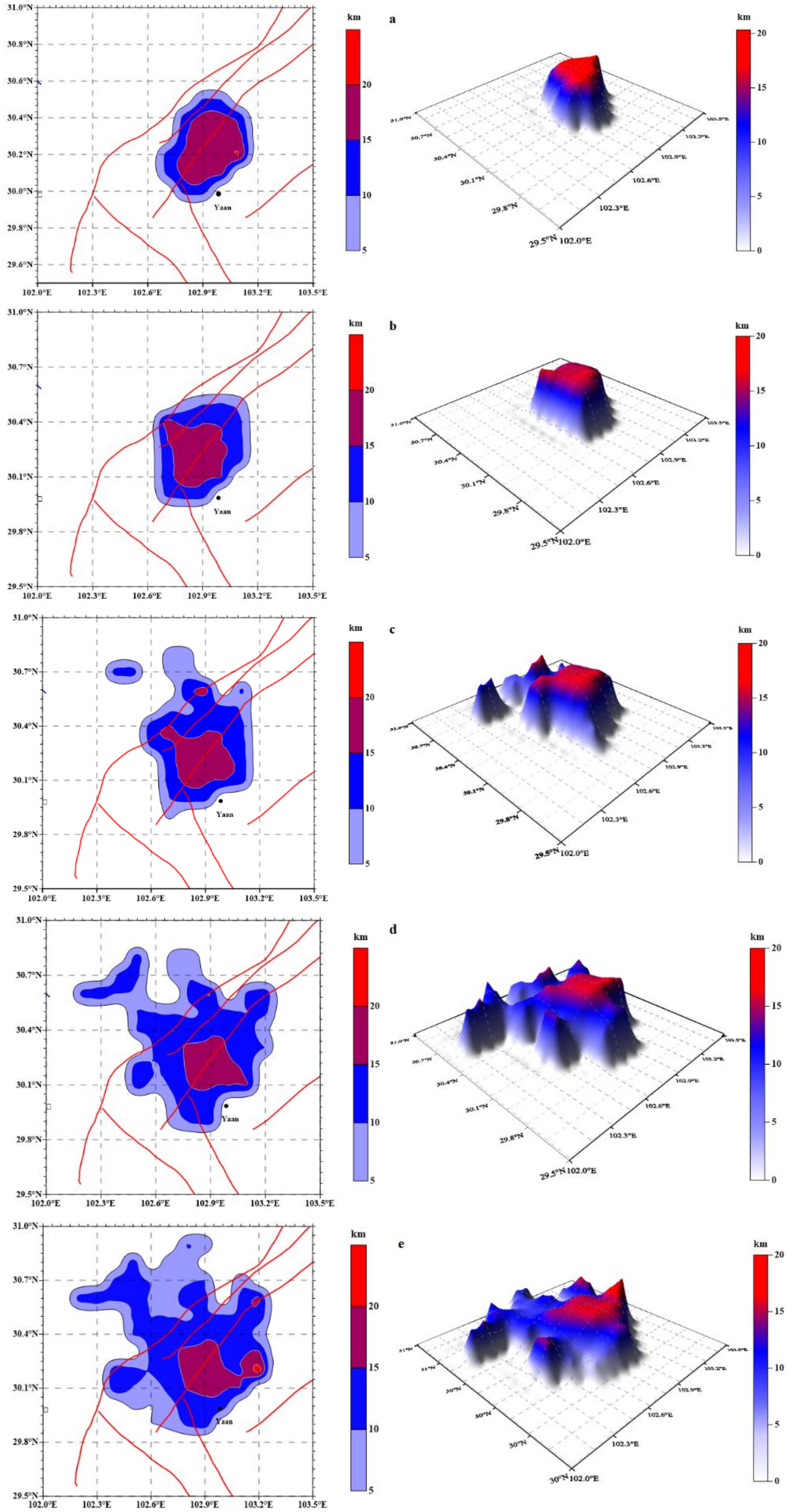

Figure 3. Spatial distribution of the focal depths of the aftershocks following the Lushan *Ms* 7.0 earthquake on the fault plane Red lines represent the locations of faults. **a** One day after the mainshock; **b** 1 month after the mainshock; **c** 5 months after the mainshock; **d** 10 months after the mainshock; **e** 2 years after the mainshock.

Table 1 The results of the *P* parameter test

Windows	ΔAIC	P_b
W_{12}	3.8	0.02
W_{23}	3.2	0.03
W_{13}	19.9	6.4×10^{-6}
L_{12}	2.6	0.03
L_{23}	4.6	0.01
L_{13}	20	5.9×10^{-6}